Transportation Geotechnics 45 (2024) 101213

Contents lists available at ScienceDirect

Transportation Geotechnics

journal homepage: www.elsevier.com/locate/trgeo

On site fouling index assessment of ballasted layers using cone dynamic penetrometer and miniature borescope image analysis

Jorge Rojas Vivanco [a,b,*], Pierre Breul [b], Aurélie TALON [b], Miguel Angel Benz-Navarrete [a], Sébastien Barbier [a], Fabien Ranvier [a]

[a] Research and Development, Sol Solution, 63204 Riom Cedex, France
[b] Institut Pascal, Clermont Auvergne University, 63174 Aubière, France

ARTICLE INFO

Keywords:
Laboratory test
Penetrometer
Geoendoscopy
Railway
Ballasted track
Fouling Index
Statistical analysis
Data fusion
Grain size

ABSTRACT

Ballast characterization is a fundamental task to optimize decision-making in maintenance or renewal programs of railway tracks. For that purpose, be able to evaluate the fouling and the deterioration of the ballast are the major problem. This study aims to characterize the fouled ballast using a Lightweight dynamic cone penetrometer (LDCP) and géoendoscope test. The methodology presented consists in analyzing the resistance properties of the ballast layer by means of dynamic cone resistance (qd) and then performing a geoendoscopy test to obtain borehole images for the material characterization. Statistical analysis of cone resistance and statistical image parameters (texture and colometry) shows their dependence on the degree of fouling as well as on its nature. As ballast fouling increases, the average cone resistance initially increases and then decreases. Images features also depend on the proportion of fouling but especially allow to distinguish different contents of fine particles in the fouling material. However, each of the measurements taken separately is not sufficient to determine a ballast fouling amount. The final results indicate that the method can accurately determine the fouling index with minimal variations.

Introduction

Context

Among the different types of railway tracks, ballasted tracks are the most widely used throughout the world. There are different types of railways tracks, in terms of materiality and structuring the most used worldwide are the ballasted tracks. This granular material has an origin of a rock which is crushed into a coarse gravel, depending on the country where it is used must meet certain requirements in the following analysis we will focus on the grain size requirements. All requirements must be met in order for the ballast layer to fulfill its functions, which include providing effective drainage, maintaining the horizontal and vertical stability of the track, lowering loads and ensuring the geometry of the track.

In the operational use of the railroad track, it is requested by the transit of trains generating dynamic and static loads. After repeated and increasing heavy loads, the ballast begins to deteriorate, losing fragments, giving rise to the fouling material. The main composition of the fouling material comes from ballast fragmentation, but there are other sources such as: Ballast breakdown, infiltration from ballast Surface, Sleeper (tie) wear; Infiltration from underlying granular layers and subgrade infiltration [23]. The fouling material modifies the mechanical behavior of the initial clean ballast and affects the functions that the granular medium must perform. The effects depend on the amount of contamination and may require extensive maintenance work. For this reason, the diagnosis and characterization of the ballasted layer is important for the safety and comfort of rail transport.

The association of lightweight dynamic cone penetrometer and geoendoscopy test (known as LDCP/geoendoscopy methodology), offers the possibility to perform railroad diagnostics based on the measurement of dynamic cone resistance (qd) and a virtual drilling composed of images of the features in depth on a continuous basis [5,16].This methodology has been used in characterization studies of clean ballast [11]and fouled ballast [22], observing the effects caused by fouling material and finding relationships between dynamic cone resistance and fouling level.

This paper presents a new methodology of characterization of the

* Corresponding author at: Clermont Auvergne University and Sol Solution, France.
E-mail address: jrojas@sol-solution.com (J. Rojas Vivanco).

https://doi.org/10.1016/j.trgeo.2024.101213
Received 5 October 2023; Received in revised form 9 February 2024; Accepted 10 February 2024
Available online 15 February 2024
2214-3912/

Table 1
Methods of fouling index determination and classification (“P4″ and ”P200″ represent the cumulative percentage of particle sizes smaller than 4.75 mm and 0.075 mm, respectively).

Classification	[23] $FI = P_4 + P_{200}$	AS 2758. $FI = P_{0.075} + P_{13.2}$
Clean	< 1	< 2
Moderately clean	1 to < 10	2 to < 10
Moderately fouled	10 to < 20	10 to < 20
Fouled	20 to < 40	20 to < 40
Highly fouled	≥ 40	≥ 45

ballast layer based on Cone resistance and image processing in order to define the fouling index and the physical properties (void ratio and grain size distribution) of the fouled ballast layer.

Fouling index assessment of ballast layer

There are different methods to determine the degree of fouling among them are Fouling index or percentage of fouling Selig (FI)[23], Percentage void contamination (PVC)[13], Void Contaminant Index (VCI)[12]and Relative Ballast Fouling Ratio (Rbf)[17].

Table 1 identifies different classification criteria according to the degree of fouling, in addition to two calculation methods, the first one proposed by Selig & Water [23]in the United States and the second one belongs to the Australian standard AS 2758.7 [4].

Each method has in common the double counting of fines due to the effects that these generate in the mechanical behavior. Moreover, each method takes into account a second component: the proportion of sands (<5 mm) for the North American method and the proportion of gravels (13,2 mm) for the Australian method.

Objective

The objective of this article is to determine the complete grain size of the ballast layer, by associating dynamic cone resistance and image analysis issues from LDCP/geoendoscopy test.

Material and methods

Material

Lightweight dynamic cone penetrometer

Lightweight dynamic cone penetrometer, hereafter instrumented LDCP [8,14], is a dynamic variable energy penetrometer which is used for soil reconnaissance, compaction control and railroad diagnostics. This device is standardized especially in France and in other countries for compaction control, for example in Chile applied in mining.

The test consists of introducing a set of steel rods equipped with a conical tip (2, 4 or 10 cm^2) into the ground by means of manual or automatic hammering. For each impact, the actuation energy in the instrumented head is measured. Other sensors simultaneously measure cone penetration. Both data are immediately transmitted to the acquisition unit and the cone resistance (qd) is calculated directly using the Dutch formula. The log of sounding, called penetrograma, plots the almost continuously in depth (z) the evolution of qd. The instrumented LDCP is a light equipment with a weight of less than 20 kg. For railway research, adaptations have been made to make it even lighter and stronger.

The calibration of the instrumented LDCP is fundamental for the determination of the density of the granular medium (ρ_d). All soils have a logarithmic model relating the dynamic cone resistance (qd) to density (see equation (1) [5]. The clean ballast model is already developed by [11], complying with the logarithmic model, he development of the experimentation is developed on the fouled ballast determining the model for different classifications of the fouling index (FI) proposed by [23].

$$\rho_d = A^{*}\ln\left(\frac{q_{d1}}{0,1013}\right) + B \tag{1}$$

where (q_{d1}) is the average dynamic cone resistance of the ballast layer and (A, B) are coefficients that depend on the fouling index.

Miniature Borescope: The géoendoscope

The géoendoscope is a miniature borescope with imaging hardware/ software used for soil characterization. With this tool it is possible to obtain detailed information on the nature of the soil, its grain size, moisture states and layer thicknesses. After instrumented LDCP test is finished, the rods are raised and another hollow rod is added, which will allow the passage of an 8 (mm) probe. Once the test is started, a continuous video is recorded, that is to say, the recording is made according to the depth and not time [9,15].

The géoendoscope images are 5 mm borehole wall width with high resolution (640x480 pixels at least). A depth recorder is added so that the video and depth are simultaneously recorded on a rugged laptop, thanks to a custom acquisition software (Fig. 1 identifies the processing of the image).

Soils used and preparation of specimens

The characterization of the soils used is shown in Table 2. Some soils are not representative of traditional railroad fouling material. For example, clays are not representative but allow us to evaluate the effects of fines, in addition to proposing a globalized model [22].The experimental procedure developed consisted of studying the grain size of the fouled ballast at different levels of fouling and density. A cylindrical metal mold with a diameter of 40 (cm) and a depth of 80 (cm) was used for this purpose. The mold size was defined from work already developed on ballast characterization [11] aiming to suppress edge effects

Table 2
Main properties of soils employed in this study.

Material / Soils	D_{max} mm	Pass. 80 µm	Pass. 2 mm	γ_{OPN} kN/m3	w_{OPN}%	AASHTO
Ballast	50	0	0	–	–	A-1-a
Sand Izeaux	5	12,9	78,2	19,5	19	A-2–4
Clay Lornage	1	50,6	97,6	20,3	18,2	A-4
Soil mixture 1	5	22,3	83,1	/	/	/
Soil mixture 2	5	31,8	87,9	/	/	/

Fig. 1. Identifies the processing of the image.

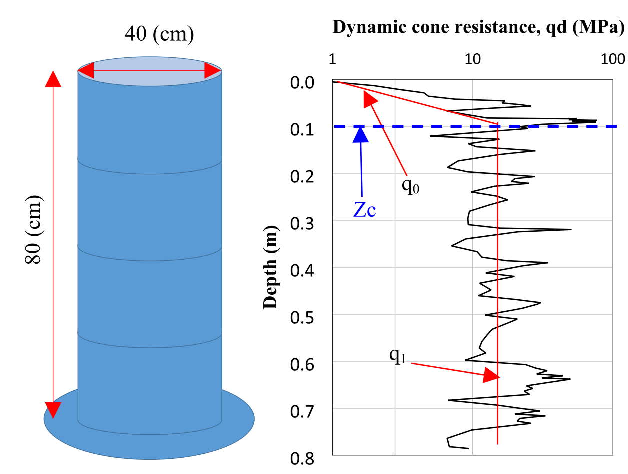

Fig. 2. (a) Mold dimensions, (b) Penetrograma type.

and to observe and develop critical strength.

This resistance becomes apparent upon surpassing the critical depth (Zc), signifying the stabilization of the cone resistance value due to soil confinement. Fig. 2 illustrates a typical penetrogram. Premature arrival at the critical depth (Zc) occurs at approximately 5 cm. The critical depth is contingent upon the degree of embedment and the compaction level employed. Higher values of these factors result in an earlier attainment of the critical depth. For each specimen, both an instrumented LDCP penetration test and an endoscopic sounding were conducted.

Sample preparation consisted of combining various proportions of clean ballast with finer material such as sand, clay or both. These mixtures were prepared in a concrete mixer and then filled into the mold and compacted at different density. In this way, it was possible to establish the correlation between the average cone resistance and the density of the granular medium (see Fig. 11A).

The density was controlled by measuring the volume of the mold, the mass of the ballast and the mass of the fouling material. Using equation (9), an approximation of the solid volume of each mold can be obtained based on the measured volume of the mold and the specific weight (the ballast and the fouling material have the same specific weight value due to their origin). The void volume is obtained by the difference between the volume of the mold and the solid volume, finally we will obtain the void ratio from equation (6).

Method

The developed calculation method primarily involves reconstructing the grain-size curve of the ballast, considering varying degrees of fouling. This reconstruction process comprises two distinct stages. The first stage entails estimating the grain-size curves for both the ballast and fouling materials. The second stage involves combining these grain-size curves based on mass estimations obtained through empirical correlations derived from laboratory experiments, which will be explained in the subsequent sections. To develop the method, it was necessary to define three states of ballast layer fouling (see Fig. 3):

Clean ballast (CB), with no fouling material between its grains,

Ballast partially fouled (BPF), a certain amount of fouling material begins to be identified in contact with the ballast grains,

Ballast completely fouled (BCF), the voids between the ballast grains are completely filled with fouling material.

It is important to distinguish between the different states, since each state will provide relevant information for the estimation of grain size curves and mass.

Estimation of the grain size of ballast and fouling material

The first phase is the estimation of the grain size curves of the ballast and the fouling material. Therefore, a specific treatment will be carried out to estimate the grain size as accurately as possible.

Clean ballast, partially fouled ballast and ballast totally fouled.

To determine the size of the ballast grains, both in their clean and partially fouled state, a semi-automatic methodology will be used in association with geoendoscopy measurements. Applying this methodology involves marking the starting and ending points of the grains, choosing those that present sizes within the range of 80 to 5 mm. These points are used as input data for a specific program that performs the calculation of the corresponding grain size distribution. To facilitate this process, customized software has been developed that provides tools designed to simplify the selection of the start and end points of each grain in an intuitive manner [6].

The virtual sieving method consists in assigning each grain to a particle size class according to the measured diameter. This results in a particle size distribution by number. This distribution is then converted into a volume particle size distribution by calculating the volume of the

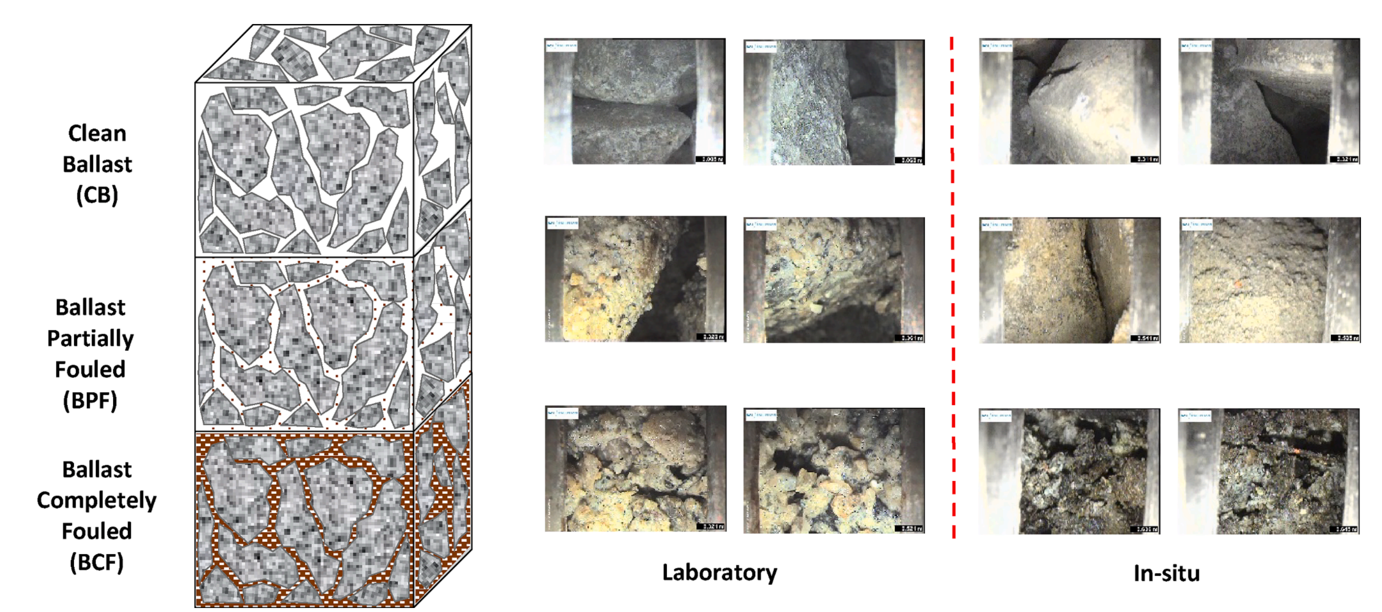

Fig. 3. Description of the condition of the ballast layer with geoendoscopy images associated with each state.

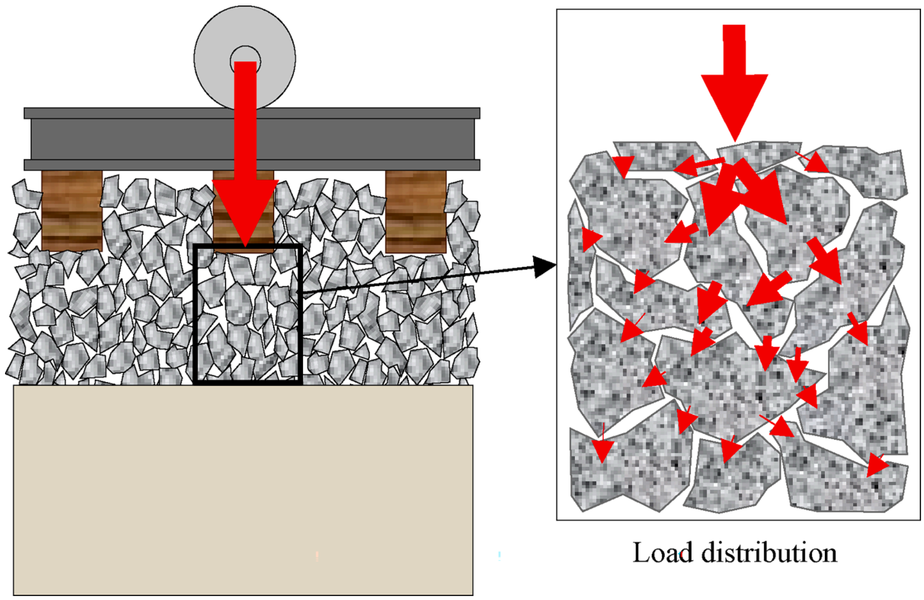

Fig. 4. Reduction of loads in depth.

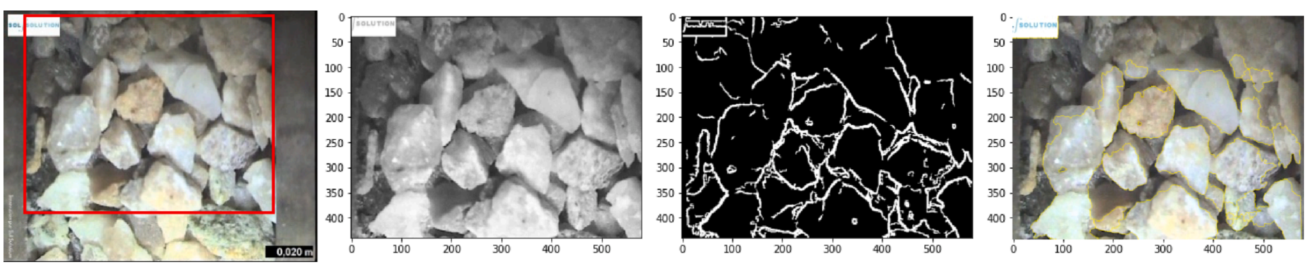

Fig. 5. Different steps of the image processing.

equivalent sphere whose diameter is the mean diameter between two sieves. This step involves a simplification of the shape of the ballast grains.

The methodology developed by Barbier [6] does not apply to the totally fouled layer since it is impossible to see ballast grains (see Fig. 3), because the voids are filled with fouling material.

To estimate the grain size of the completely contaminated ballast layer, we formulate the following hypothesis: "The grain size of the ballast in the clean and partially contaminated states reflects that of the completely contaminated ballast." From a more theoretical standpoint, we can observe a decrease in the loads (reduction with depth) in Fig. 4. Therefore, we can conclude that at greater depths, the ballast is in a less degraded state.

Fouling material.

The above method could be applied to the fully soiled layer, but the measurement process would be very time consuming due to the large amount of grains. For this case, an automated analysis is performed using algorithms developed in Python.

The algorithm starts with starting with the identification of the analysis area on the image (see Fig. 5). The processing loop starts with the conversion from RGB (red, green, blue) to HIS (hue, saturation, intensity). Subsequently, a morphological erosion of the image is generated to generate the extraction of the contour of the grains from Gaussian filters recovering the minimum and maximum values of the image pixels corresponding to 0 and 255. The final treatments are geodesic dilation by a square following a 2D scheme of 4 connections, obtaining the external gradient with a square structuring element and threes holding to a new image.

Relationship of the grain size curves from mass estimation

Soil grain size is the statistical distribution of the sizes of the grains and particles that make up the granular medium. By sieving it is possible to determine the partial mass percentages obtained by each sieve. By means of simple mathematical operations it is possible to represent the grain size curve based on the accumulated percentage of the sieves.

In our specific application, we obtain grain size curves for both the ballast and the fouling material. However, there is no simple method to combine both grain size curves. For this reason, the use of correlation factors from the masses is proposed. For example, two different soils "A" and "B" are to be mixed. For each soil we know its particle size ($\%P_n$) and the amount of mass to be mixed (M). The grain size of the mixture would be calculated as shown in equation (2), where from correlation factors multiply the cumulative mass percentage of each sieve.

$$\%P_n(A+B) = \%P_n(A)^*F_A + \%P_n(B)^*F_B \tag{2}$$

$$F_A = \frac{M_A}{M_A + M_B} \tag{3}$$

$$F_B = \frac{M_B}{M_A + M_B} \tag{4}$$

where $\%P_n$ is the mass percentage for sieve n (from 63 mm to 80 μm), F is the coupling factor obtained as a function of the mass of each material and M is the amount of mass for each material.

As indicated, the correlation factors are the key to the coupling of the grain-size curves. Fig. 5 shows the dissociation of materials that compose the ballast layer, in mass units. The following sections will show how the volume and mass of each material is estimated.

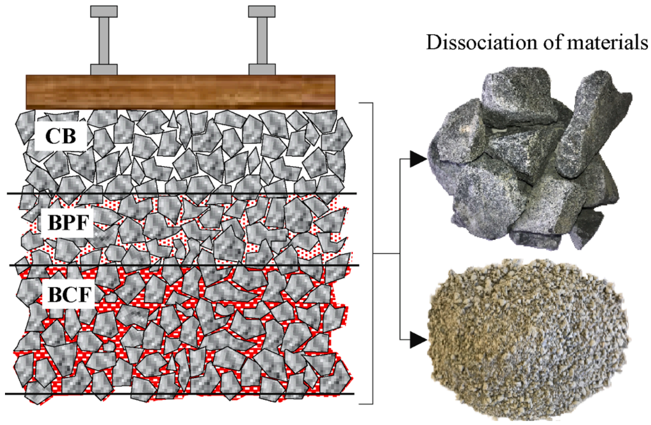

Fig. 6. Dissociation of the ballast mass and the fouling material.

Clean ballast.

The first phase of ballast mass estimation consists of determining the volume of ballast in the granular medium. In equation (5) we identify that the total volume (V_T) will be composed of the ballast volume (V_B) plus the void volume (V_V). From classical Geotechnics, the relationship of void ratio (e) with the volume of voids and solids is proposed (see equation (6). In the case of wanting to estimate the volume for one cubic meter of material, it is possible to determine the volume of ballast with equation (7). The estimation of the void ratio is obtained from equation (8), which is related to the density of the granular medium (see Fig. 10).

$$V_T = V_V + V_B \tag{5}$$

$$e = \frac{V_V}{V_B} \tag{6}$$

$$V_B = \frac{1}{1+e} \tag{7}$$

$$e = 0,0027(\rho_d)^{2}* - 0,1989*\rho_d + 3,1467 \tag{8}$$

The ballast mass estimate (m_B) is related to the specific weight of the ballast (γ_B) which is usually 26 kN/m^3. The equation shows the relationship between the volume and specific weight of the ballast to determine the mass of the ballast (see equation (9).

$$m_B = \gamma_B * V_B \tag{9}$$

Partially fouled ballast.

This layer has two components, the ballast and the fouling material. The ballast mass will be calculated in the same way as in the previous case, the value will be corrected from the thickness of the layer.

The case of the fouling material is different, as it is in the form of a coating on the ballast grains (see Fig. 6). To estimate the volume of the lining, the quantity of ballast grains must first be calculated according to their particle size and the volume calculated above, using an average diameter for each sieve as an assumption. An expert will determine the thickness of the coating, values from 1 to 6 mm were observed in the laboratory. With the value of the coating it is possible to calculate a new volume according to the new diameter (D_f), this volume will be multiplied by the amount of grains previously. The final volume of fouling material is calculated with equation (10), which shows the process described above.

(Fig 7.)

The mass of this clogging material will be estimated according to Equation (9), but substituting a loose density of 13 kN/m^3 for the specific gravity.

$$\Delta V_F = \left(\sum N_i * \frac{\pi}{6} * \left(D_{f(i)}\right)^2\right) - V_B \tag{10}$$

Ballast completely fouled.

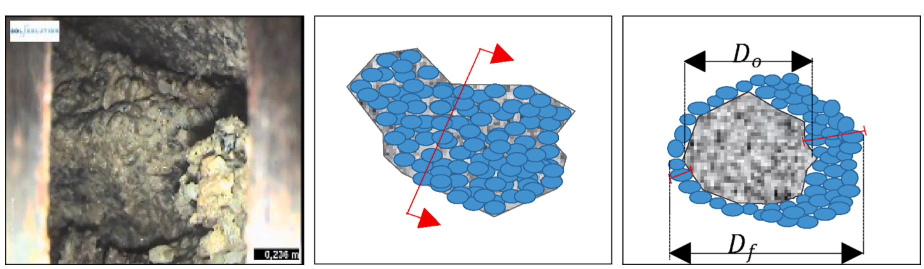

Fig. 7. Effect of fouling material coating.

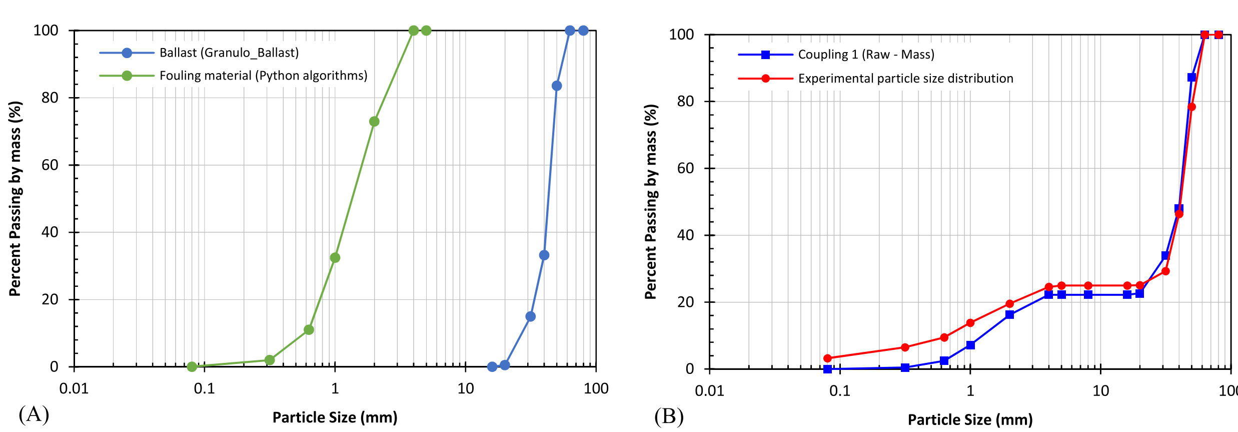

Fig. 8. (A) Grain size curve estimation from the Granulo_ballast program and Python algorithms and (B) Comparison of particle size distribution between experimental result and image processing analysis (Coupling 1).

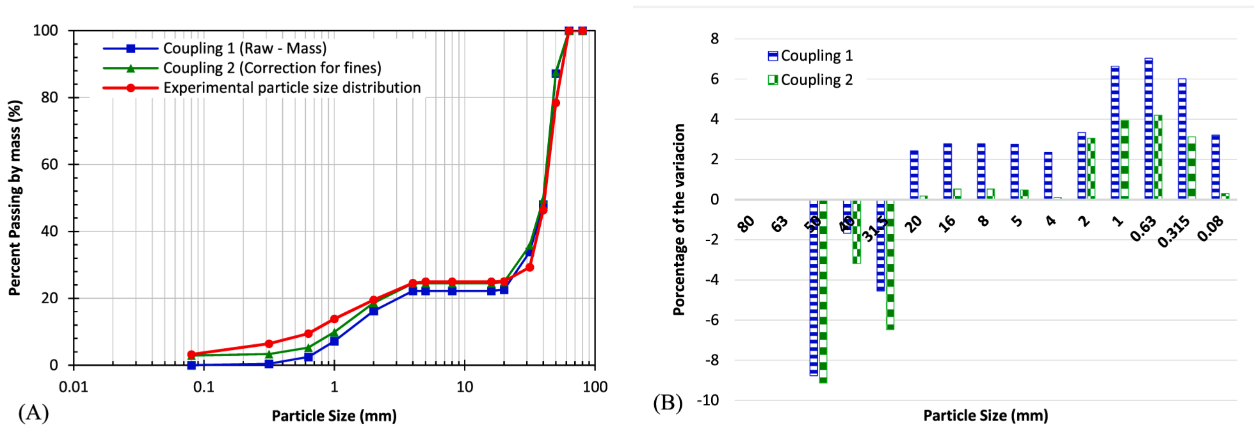

Fig. 9. (A) Results of the different couplings, (B) Type 1 and 2 coupling variability.

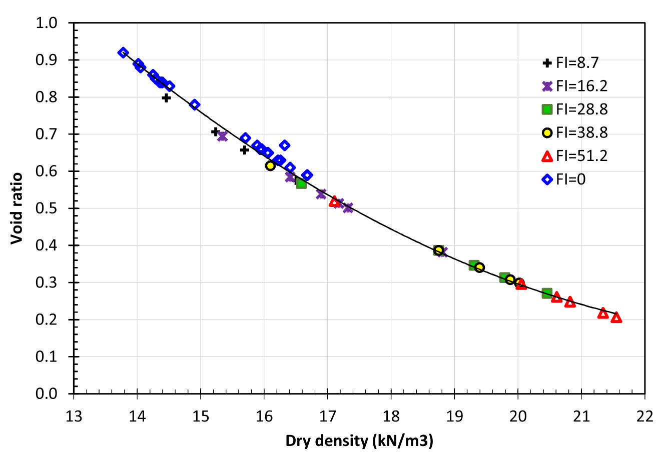

Fig. 10. Relation between density and void ratio.

The ballast mass of the fully embedded layer shall be estimated from the clean ballast and corrected for the height of the layer. The volume of the embedding material shall be equal to the void ratio volume. The void ratio shall be estimated from equation (8).

The estimation of the mass shall be made by multiplying the calculated volume by the density of the embedded material. The laboratory measured density value is [17; ± 3] (kN/m^3). The variability of the density will depend on many factors, especially the years of operation and the amount of traffic.

Curve coupling

The coupling of the curves is based on the mass of the components. Once the mass is obtained, the coupling factors of equations (3) and (4) are calculated and then coupled using equation (2).

Fig. 8A presents the grain size curves derived in laboratory from image analysis of a LDCP/geoendoscopy test. The test was carried out in a reconstituted soil sample mixing clean ballast and sand, respectively. This sample is not intended to be representative of the grain sizes found in the track on ballast, but to test the method presented in a soil with a large distribution and including a size discontinuity. The mass of each element was estimated, obtaining participation factors of 22.2 % for the fouling material and 72.8 % for the ballast. The results of coupling 1 are shown in Fig. 8B. Up to 20 mm, the results of coupling 1 show a trend similar to the particle size used in the laboratory; above 20 mm, an average deviation of 4 % is observed.

Curve correction

Variability in mass-based coupling can experience significant fluctuations in the range of 2 mm to 80 µm, and these fluctuations can be

Table 3
Main properties of soils employed in this study.

Classification	Coefficient “A”	Coefficient “B”
Clean	1,716	11,57
Moderately clean	1,702	11,59
Moderately fouled	2,907	9,65
Fouled	1,970	14,30
Highly fouled	1,335	17,60

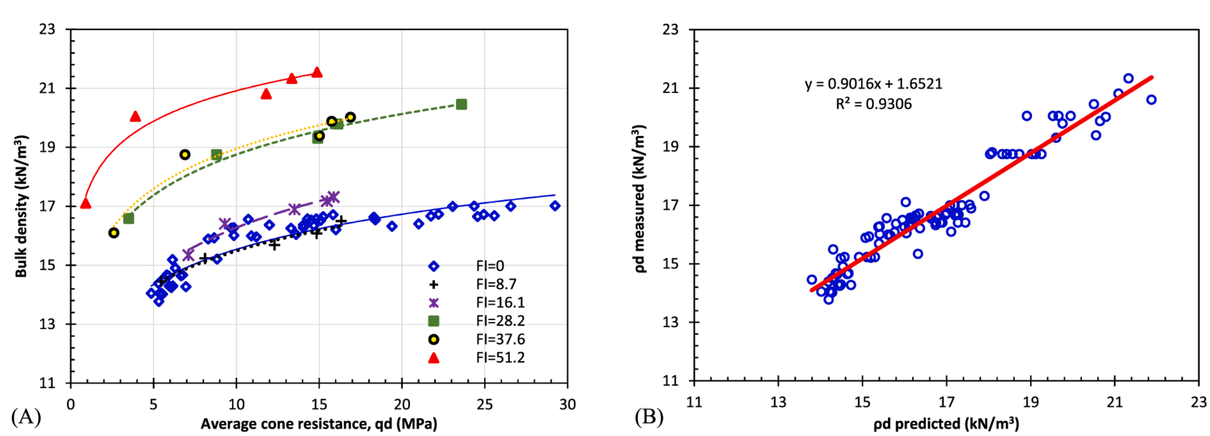

Fig. 11. (A) Relation between average cone resistance and density and (B) Linear regression of results.

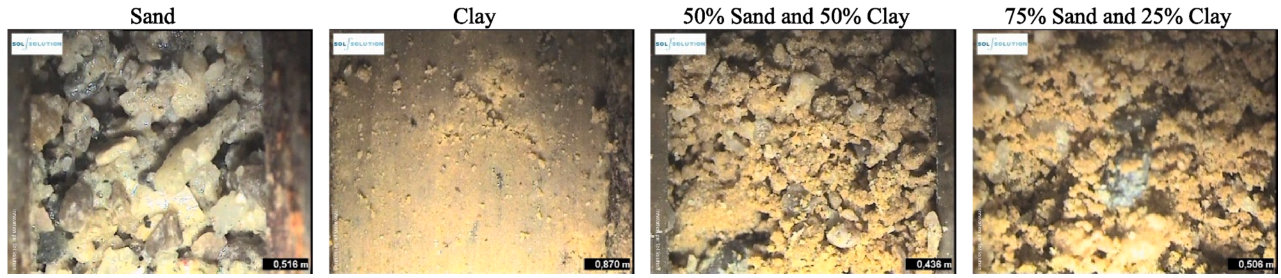

Fig. 12. Fouling materials evaluated to establish a relationship between imaging parameters and the mass percentages associated with the fouling index (P4 and P200).

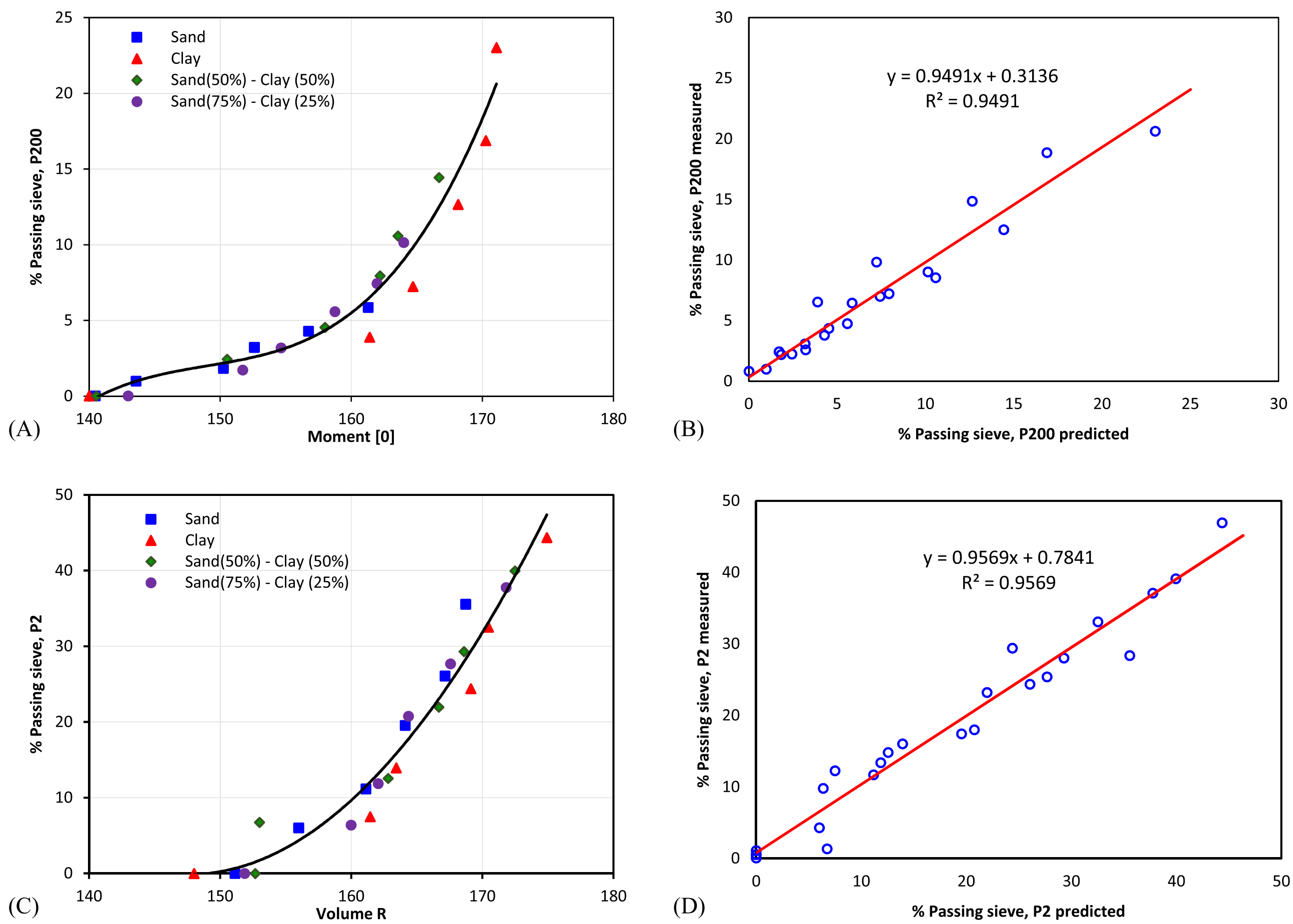

Fig. 13. (A) Relation between Moment [0] v/s % Passing sieve, P200, (B) Linear regression for Moment [0], (C) Relation between Volume R v/s % Passing sieve, P2 and (D) Linear regression for Volume R.

affected by several factors, such as the representativeness of the data relative to the granular media, humidity levels, image quality and brightness.

To reduce the difference between the experimental curve and the results obtained by coupling, the percentage of fines that have not yet appeared in the first results will be incorporated. To incorporate the percentage of fines, a sensitivity study was carried out on different texture and colometry parameters of the geoendoscopy images, which are sensitive to the content of fines and sands [9,15]. A total of 13 parameters were analyzed, the most capable of representing the estimate are (see Fig. 12) [21]:

Moment [0] (M[0]) for fines estimation is a texture parameter based on the highest frequency calculated by the Fourier transform, which shows that it is possible to characterize the soil as a function of texture [10].

Volume R for sand estimation. This is a colometry parameter capable of quantifying the amount of red color recorded.

The percentage of fines of the entire ballast layer is estimated with equation (11), which depends on the average value of the entire ballast layer (BS + BPF + BCF). The correction of the first coupling is made by incorporating the percentage of fines, which will be counted as a new mass percentage to the previously calculated, this will allow the initial grain size curve to approach the experimental one. Equation (12) shows how to correct the values for each sieve.

$$\%C_{80\mu m} = 2*10^{-14}*e^{0.2039*\overline{M[0]}} \quad (11)$$

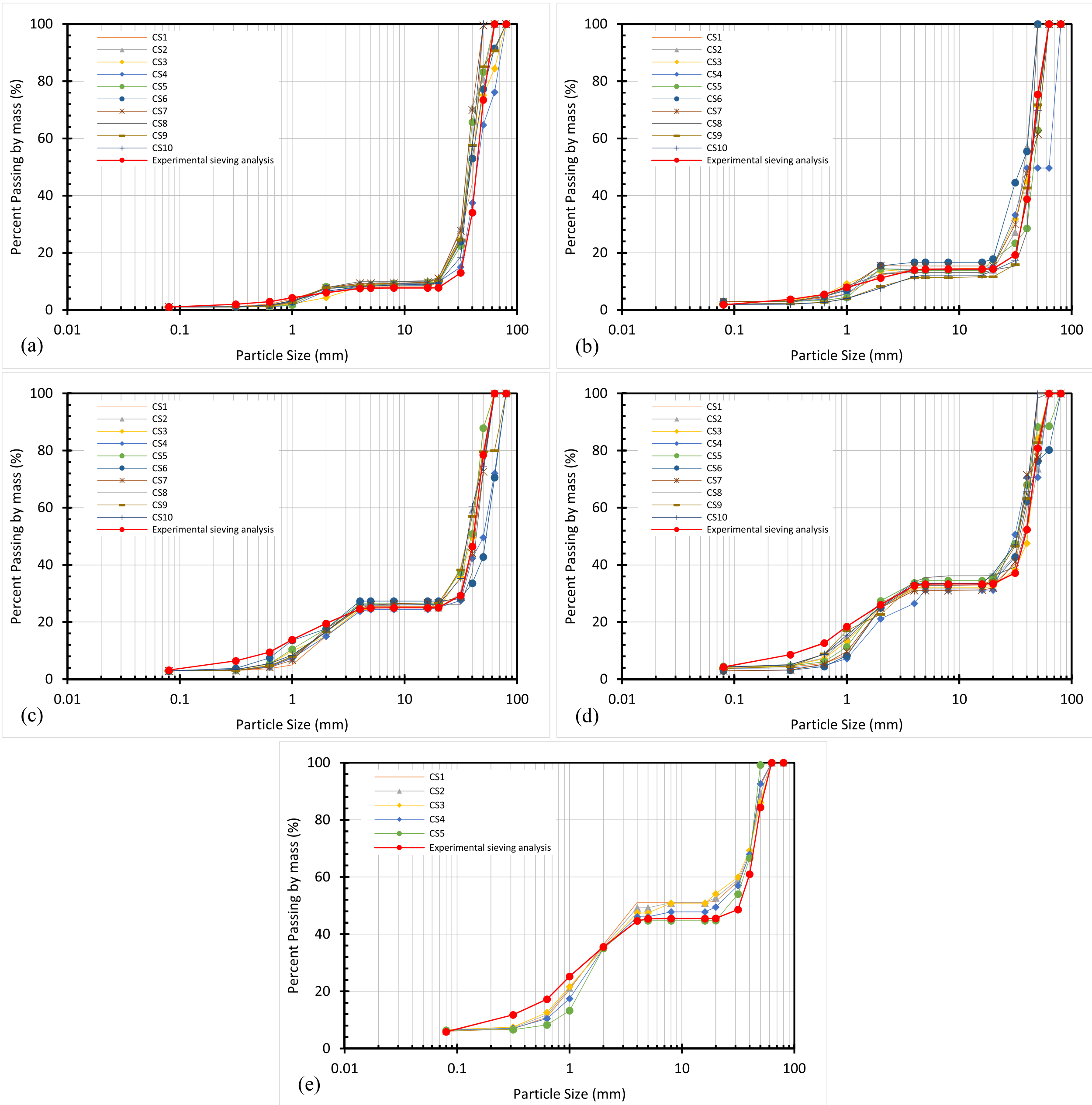

Fig. 14. Laboratory grain size coupling results (a) FI = 8,6%, (b) FI = 16,2%, (e) FI = 28,2%, (d) FI = 37,6% and (e) FI = 51,2% (CS = Coupling of sounding, The number indicates the test performed).

$$\%P_{n(C2)} = P_{n-1(C2)} - \frac{P_{n-1(C1)} - P_{n(C1)}}{100 + \%C_{80\mu m}} \quad (12)$$

Fig. 8A shows the result of type 1 coupling, which uses the mass coupling factor, and type 2, which performs a correction based on the estimated percentage of fines. The proposed couplings give good results, as can be seen in Fig. 9A, although variations remain. From 20 (mm) to 80 (μm) a reduction of at least 4 % is achieved (see Fig. 9B).

Results

Assessment of density, void ratio and dynamic cone resistance (qd)

Fig. 10 shows the relation between density and void ratio for clean ballast and ballast with different states of fouling index (FI). The density of the granular medium will allow us to know the void ratio, a fundamental parameter for the proposed calculation methodology.

Initially, a universal model of soils relating density to dynamic cone resistance was established as shown in Equation (1). This relationship can be extending for each fouling state of the ballast as shown in the Fig. 11A. All the curves have the same trend, but as the fouling increases, we observe the vertical displacement of the curves due to mass incorporation.

Fig. 11B shows the results of a linear regression between density, dynamic cone resistance and fouling index. Where “x” is the prediction of the results and “y” is the laboratory measured. Table 3 presents the essential coefficients for the determination of the density of the granular medium at various fouling levels. These coefficients are essential for their substitution in the corresponding Equation (1). The values reported here were obtained by means of a rigorous analysis of logarithmic trend curves, using a scientific and statistical approach.

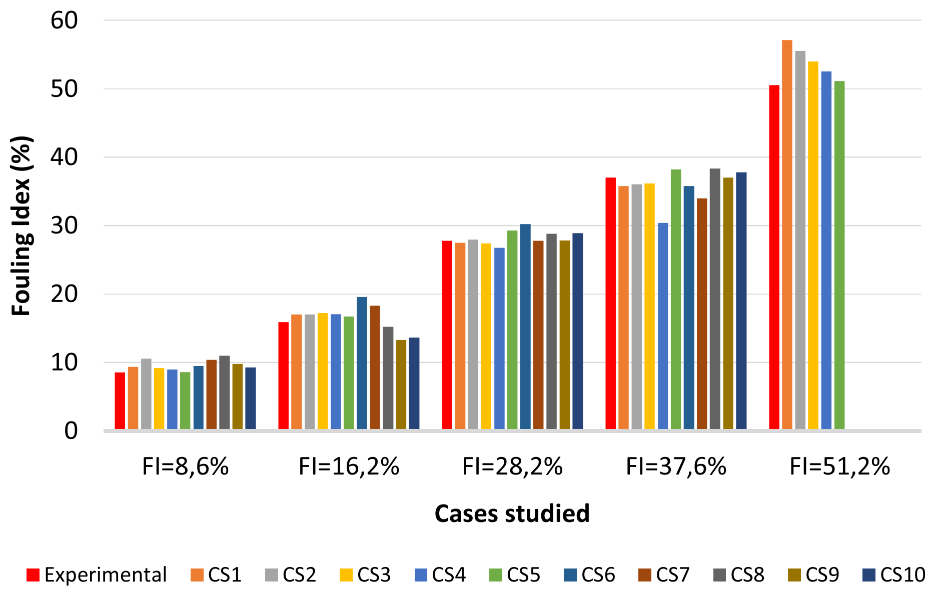

Fig. 15. Comparative analysis of fouling index estimation.

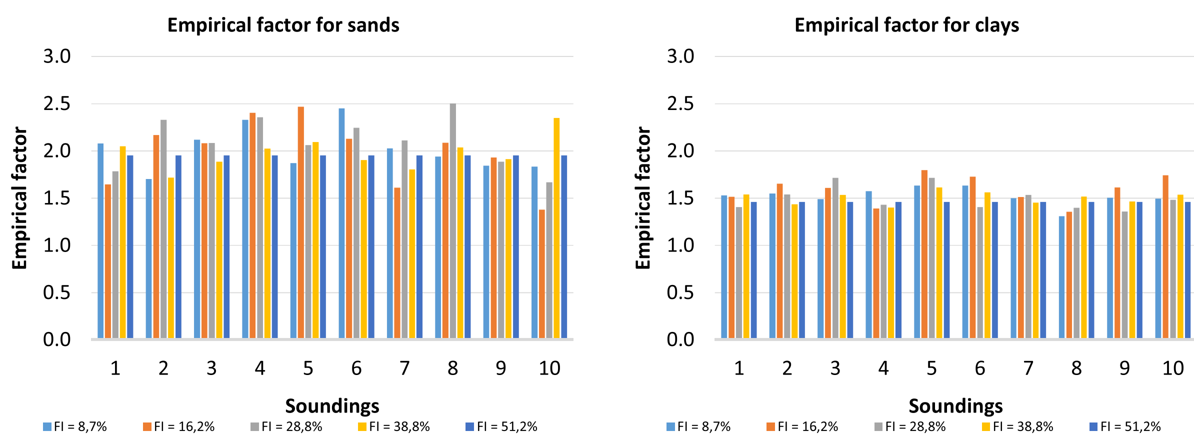

Fig. 16. Estimation of the empirical ratio factor for sands and clays.

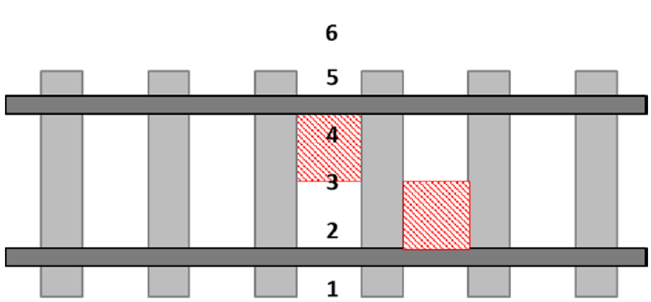

Fig. 17. Distribution of soundings in the railway and zones where the samples were taken.

Assessment of grain size features by images analysis

This evaluation is carried out so that the fines are incorporated in the coupling of the grain-size curves. As indicated above, an analysis of thirteen different parameters was carried out, of which there were two protagonists. The analyzed images of the ballast layer were the partially and totally fouled layer. For this purpose, the same fouling materials proposed by [22] were used (see Fig. 12). As [9]highlights, it is crucial to take into account the inherent limitations of various soil types. Consequently, an analysis was conducted to examine the behavior of different parameters concerning the values associated with sands (2 mm), fines (80 μm), and the fouling index (FI).

The texture and colometry parameters obtained are associated with the fines (80 μm) and sands (2 mm) content of the granular medium. Obtaining universal models (applicable to different types of fouling material) for both cases using texture and colometry parameters.

The model obtained for the texture parameter "Moment [0]" is coupled with the fines content defining a polynomial model. In the initial part of the model, sands with rough textures are identified, while in the final part of the model, smoother textures are identified (see Fig. 13A). In addition, a good correlation is observed between the percentage of sands and the colorimetric parameter "Volume R", that is responsible for accounting for the red color content in the image (see Fig. 13C). However, when considering a greater diversity of soils, it is possible that this relationship does not maintain the same trend in other sands and may be specific to the set of samples analyzed. Consequently, this relationship is not considered in the calculation of the particle size. Finally, the combination of the models is related to the heights of the

Fig. 18. (a) Profile of the studied ballast layer and (b) Endoscope images linked to the ballast profile.

partially and fully embedded ballast layers.

Assessment of grain size distribution

General analysis of results

Fig. 14 shows the results of the different fouling states. For the 5 cases shown, it can be observed that the estimates have a similar trend to the laboratory control. In the first instance, the correlation method between ballast mass and fouling material gives good results.

The first one is the grain size curves of inputs, if these curves do not have a good representation is where variability is generated for each sieve. The second is mass estimation, which depending on its effectiveness may increase or minimize the errors of the input curves. Finally, the coupling error is closely linked to the amount of fouling material. In all cases, variations are found with respect to the laboratory-controlled curve, but this is maximized as a function of the amount of fouling material. For example, an average error for the moderately clean state is [2 %; ±1] and in the very fouled state it is [7 %; ±4].

From the grain size curve obtained from the coupling, the fouling index proposed by Selig and Waters [23] can be calculated. Fig. 15 shows a comparative analysis of the experimental grain-size curve and the LDCP/geoendoscopy test. Some variability in the results is observed due to factors explained in previous paragraphs.

Discussion of variability of results

Variability exists because of the representativeness of the catch [20], If what is captured is not representative, it does not mean that the results are erroneous since they are closely related to what is captured. For this reason, there are regulations which determine the minimum mass for the results to be representative of the granular medium. In France the ballast must comply with the following standards to be used NF NR 13450 [3] and NF EN 993–1 [2]. For example, the NF EN 993–1 [2] standard requires a minimum quantity of 80 (kg) for a maximum size of 90 (mm). Obtaining a linear trend curve, we calculate that for a maximum size of 63 (mm) it is necessary to have 47.5 (kg) to be representative and that is equivalent to at least 75 grains of ballast. Normally in a laboratory or field endoscopic test about 20 grains are identified on average (this varies depending on the thickness of the layer). Consequently, the capture of an endoscopic test is not representative for the clean and partially soiled ballast layer and could have consequences on the accuracy of the results. It should be noted that normally in a diagnostic campaign many tests are performed and these could be coupled to be representative of the granular medium and be accurate in the results delivered. In the case of fouling material, the NF EN 993–1 [2] standard requires 600 (gr) and the NF94-056 [1] standard 300 (gr) of material with a maximum diameter of 5 (mm) in order to have the necessary representativeness. Consequently, for the case of fouling material, it is easy to arrive at representativeness.

The effect of humidity on the fouling material. Although we worked with a humidity between 5 and 8 %, it is important to carry out new tests to establish the effects of water on image processing and dynamic cone resistance. Because saturations equal to 100 % can be observed in field measurements.

Although the method provides good results with a general average accuracy of 3,5% of sieve variability from 20 (mm) and above, it is important to establish that the tolerable percentage must be defined by each agency in charge of the design, operation and maintenance of the railway. This is due to the fact that the high variability of the ballast can lead to an underestimation or overestimation of the degree of ballast soiling, which can result in high costs. For example, in the case of overestimation, it would generate more costly ballast cleaning cycles and a reduction of the useful life; in the case of underestimation, it would result in deformations or failure of the railway [18].

Estimation of the fouling index by thickness measurements

Based on the laboratory results, we propose the following estimation of the fouling index from the thicknesses of the different ballast layer states:

$$\%FI = \frac{H_{sc}}{R^{*}H_{BC}} \tag{13}$$

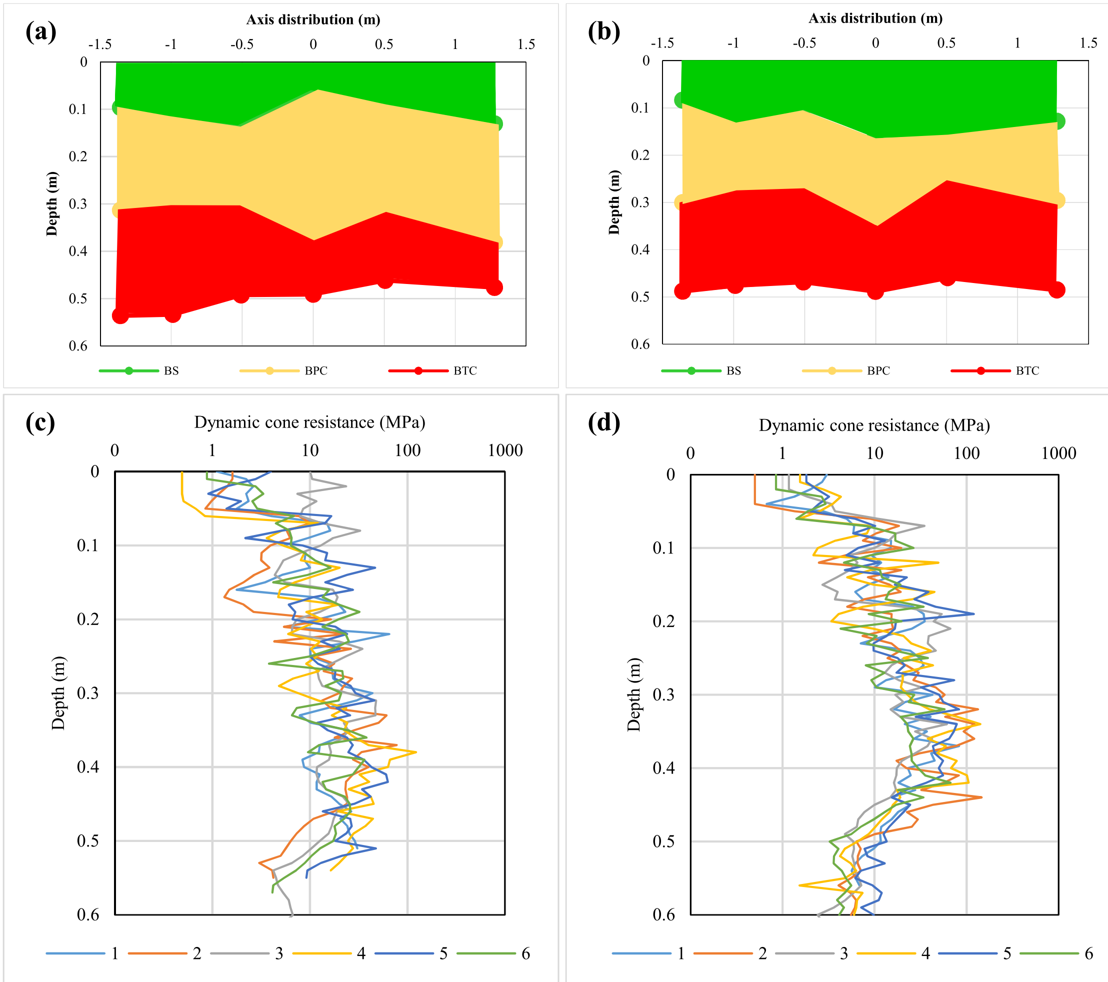

Fig. 19. (a) Thickness distribution of the different ballast states at site 610, (b) Thickness distribution of the different ballast states at site 630, (c) Penetrogram results for site 1 (610) and (d) Penetrogram results for site 2 (630).

where H_{SC} is the thickness of the ballast layer having the full void ratios of pollution material, H_{BC} is the thickness total of the ballast layer and R is an empirical relationship obtained in the laboratory (For sands ≈ 2 and for clays ≈ 1,5).

Fig. 16 shows the estimation of the factor of fifty LDCP/geo-endoscopy tests for sands and clays. As indicated by [7,22]the compaction method could generate variations in this approximation simply by increasing the compactness of the fouling material.

Validation by evaluation of a study site

The validation of the method was carried out on the French railway network, specifically at kilometer points 465 + 610 (Site 1: 610) and 465 + 630 (Site 2: 630). Fig. 17 shows the distribution of the LDCP/geoendoscopy test and the areas where the samples were taken (area marked in red). For each LDCP/geoendoscopy test, two endoscopies will be taken, for the second one the bar will be rotated 180 degrees.

In Fig. 18 is a picture of the profile of the ballast layer at site 2 (630) associated by endoscope images as a function of depth. A large amount of pollution and degradation of the layer can be observed.

Based on the results of the LDCP/geoendoscopy test, the profile of the ballast layer can be plotted, determining the three states proposed in this article: clean ballast (BS), partially fouling ballast (BPF) and totally fouling ballast (BCF) (see Fig. 19). By means of the thickness distribution, it can be identified that site 2 (630) has a higher percentage of fouling material.

The mechanical characterization of the site was carried out using instrumented LDCP, the results are shown in Fig. 19 and we can conclude: (i) The mechanical resistance of the track on a transverse axis is not the same; (ii) The highest dynamic cone resistance results are concentrated in the sectors near the rails; y (iii) With the above points we identified that the mechanical resistance increases when there is a tolerable level of clogging, experimental studies support this point [7,19,22]; (iv) Following the same logic, we can globalize the results and indicate that the mechanical resistance of site 2 (630) is higher because it has higher levels of fouling.

The results proposed by this methodology to obtain the particle size of the railway ballast are shown in Fig. 20. Results from 1 to 6 represent the first measurements obtained by geoendoscopy. On the other hand, results 101 to 106 are the additional measurements made by rotating the endoscopic rod 180 degrees. The individualized analysis for each borehole shows a variability finding results above and below the curve obtained by the laboratory, this is due to the fact that the thickness distribution is not homogeneous and to a great extent is an important parameter for the methodology. With all the results it is possible to determine a grain size curve according to weight weights estimated by the methodology, identifying a modification of the grain size curve obtaining a distribution almost similar to the one obtained in the laboratory. The results show a similar variability to those obtained in the laboratory.

Table 4 shows that the results obtained through the calculation method exhibit a remarkable consistency, revealing values close to the

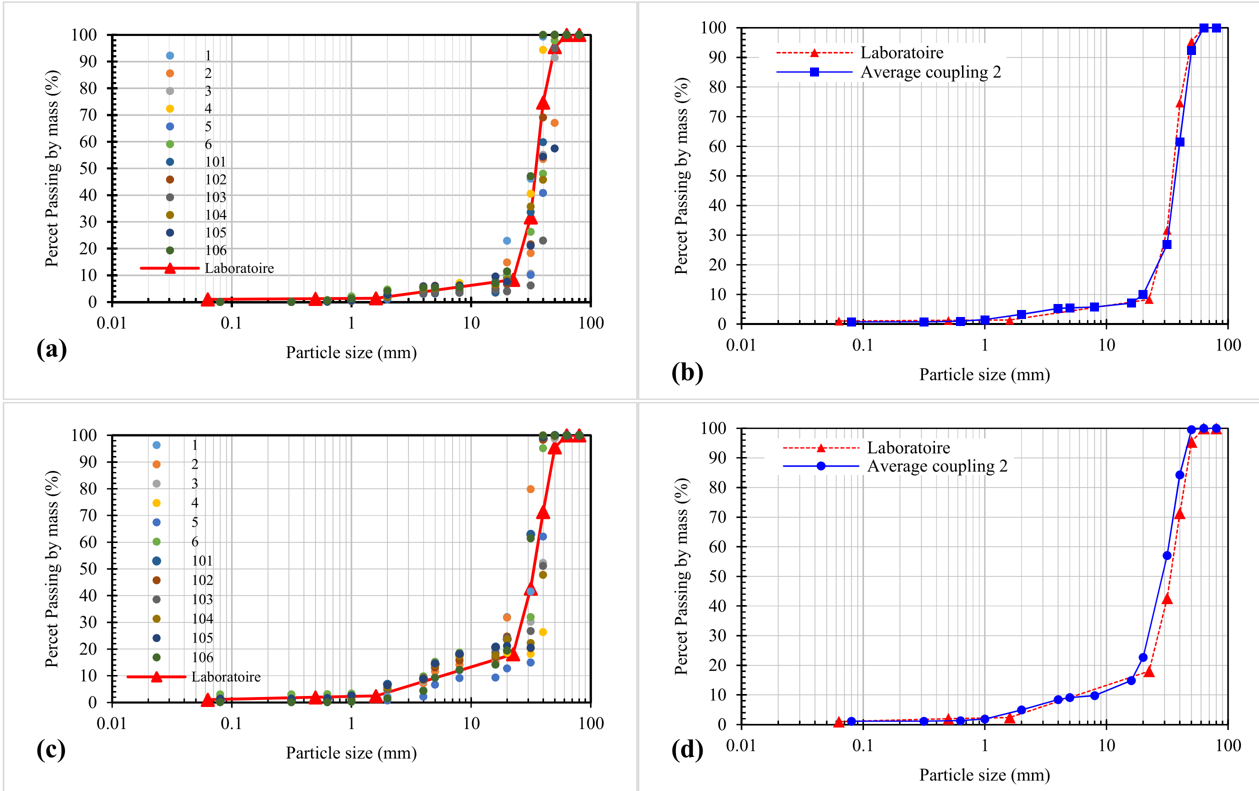

Fig. 20. (a) Results of the grain size distribution for each sounding of site 1 (610); (b) Average result of the grain size distribution of site 1 (610); (c) Results of the grain size distribution for each sounding of site 2 (630); (b) Average result of the grain size distribution of site 2 (630).

Table 4
Estimation of the fouling index (Selig and Waters).

Site	Measure	Grain size estimation	Estimation from thicknesses
610	6,10	6,15 [±1,28]	4,34 [±3,57]
630	10,01	9,66 [±1,85]	11,61 [±5,02]

average with moderate variability, as suggested by the standard deviation. In contrast, in the case of the estimation based on thicknesses, although there is a tendency for the average value to be close to the reference value obtained in the laboratory, a more marked variability is observed, reflected in a wider standard deviation.

Conclusion

Effective asset management in railways infrastructure is essential to ensure safe and efficient operation. In particular, accurate assessment of ballast layer grain size is critical to the safety and performance of the railway. The methodology based on the coupling of instrumented LDCP and geoendoscopy test, has been developed as a valuable tool to obtain this information without the need for invasive interventions.

The LDCP/geoendoscopy methodology is based on two main processes: obtaining grain size curves for ballast and embedding material, followed by their coupling by means of relationships between the mechanical and physical properties of the granular medium. This allows the estimation of additional parameters, such as density and void ratio. The process is applied considering the geotechnical composition of the railway and requires a careful approach to image acquisition, processing and analysis.

The results obtained in the laboratory and in situ demonstrate excellent agreement with the grain sizes obtained in the laboratory, albeit with variations associated with each sieve size. The variability is attributed to several factors, including the representativeness of the probe measured by the endoscope, the number of tests performed and the cross-sectional location. Despite these variations, the LDCP/geoendoscopy methodology offers a valuable alternative to conventional sampling methods, saving time and reducing the need for invasive interventions.

Importantly, the variability in results is influenced by several factors, suggesting the need for continued evaluation and refinements in the methodology. Future research could focus on improving the accuracy and robustness of the image acquisition and analysis process. In addition, considering a larger number of tests could reduce variability. The long-term outlook is for the LDCP/geoendoscopy methodology to become a standard tool in rail asset management, optimizing resources and improving decision making in track infrastructure.

CRediT authorship contribution statement

Jorge Rojas Vivanco: Conceptualization, Methodology, Validation, Formal analysis, Investigation, Data curation, Writing – original draft, Writing – review & editing. **Pierre Breul:** Validation, Writing – review & editing. **Aurélie TALON:** Validation, Writing – review & editing. Miguel Angel Benz-Navarrete: Conceptualization, Methodology, Validation, Writing – review & editing. **Sébastien Barbier:** Validation, Writing – review & editing. **Fabien Ranvier:** Validation, Writing – review & editing.

Declaration of competing interest

The authors declare that they have no known competing financial interests or personal relationships that could have appeared to influence the work reported in this paper.

Data availability

The data that has been used is confidential.

References

[1] AFNOR. NF P 94-056 - Analyse Granulométrique - Méthode par tamisage à sec après lavage 1996:16.
[2] AFNR. NF EN 993-1 Essais pour déterminer les caractéristiques géométriques des granulats — Partie 1 : Détermination de la granularité — Analyse granulométrique par tamisage 2020.
[3] AFNR. NF RN 13450 - Granulats pour ballasts de voies ferrées 2003:40.
[4] Austroads. AS 2758.7—1996 Aggregates and rock for engineering purposes Part 7 : Railway ballast 1996.
[5] Barbier S, Haddani Y, Sastre-jurado C, Benz-navarrete M. Mise Au Point D'Une Methode Automatique Pour La Determination Des Proprietes Geomecaniques De Sols in-Situ a L'Aide Du Pandoscope®. Journées Natl Géotechnique Géologie l'Ingénieur – Champs-Sur-Marne 2018 MISE 2018:1–9.
[6] Barbier S, Haddani Y, Saussine G, Benz-Navarrete MA. In situ determination of the particle size distribution of ballasted layers by PandoScopic® image analysis. Symp Int GEORAIL 2017;2017:215–26.
[7] Barbier S, Rojas Vivanco J, Benz Navarrete MA, Haddani Y. On the influence of ballast fouling materials and compaction states on the dynamic cone resistance. Railw 2022 - Proc Fifth Int Conf Railw Technol Res Dev Maint 2022:1–6. 10.4203/ccc.1.20.9.
[8] Benz-Navarrete MA, Breul P, Bacconnet C, Moustan P. The PANDA®. Variable Energy Lightweight Dynamic Cone Penetrometer: A quick state of art. ASTM; 2020. p. 1–12.
[9] Breul P. Caracterisation Endoscopique Des Milieux Granulaires Couplee a L'Essai De Penetration. Université Blaise Pascal – Clermont II, 1999.
[10] Breul P, Gourvès R, Boissier D. In situ granular materials characterisation using endoscopy. Proc Geovision'99, Int Symp Imaging Appl Geol 1999:25–8.
[11] Breul P, Saussine G. On site mechanical characterization of the ballast state. Period Polytech Civ Eng 2011;55:31–8. https://doi.org/10.3311/pp.ci.2011-1.04.
[12] Bruzek R, Stark TD, Wilk ST, Thompson HB, Sussmann TR. Principles of Degraded Ballast and Their Track Safety Implications. **2016 Jt. Rail Conf. JRC** 2016, 2016. 10.1115/JRC2016-5725.
[13] Feldman F, Nissen D. Alternative testing method for the measurement of ballast fouling: percentage void contamination. Conf Railw Eng 2002:101–11.
[14] Gourvès R, Barjot R. Le pénétromètre dynamique léger PANDA, The PANDA ultralight dynamic penetrometer 1992.
[15] Haddani Y. Caractérisation et classification des milieux granulaires par géoendoscopie. Clermont II: Université Blaise Pascal –; 2004.
[16] Haddani Y, Breul P, Saussine G, Navarrete MAB, Ranvier F, Gourvès R. Trackbed mechanical and physical characterization using PANDA®/Geoendoscopy coupling. Procedia Eng 2016;143:1201–9. https://doi.org/10.1016/j.proeng.2016.06.118.
[17] Indraratna B, Su LJ, Rujikiatkamjorn C. A new parameter for classification and evaluation of railway ballast fouling. Can Geotech J 2011;48:322–6. https://doi.org/10.1139/T10-066.
[18] Ionescu D. Ballast Degradation and Measurement of Ballast Fouling. 7th Railw Eng Proc 2004:169–80.
[19] Kang M, Wang H, Qamhia IIA, Tutumluer E, Haddani Y, Bankston A. Degraded ballast stiffness characterization using bender element field sensor and PANDA ® penetrometer. TRB Annu Meet 2023;2677(8):428–38.
[20] Kumara GHAJJ, Hayano K, Ogiwara K. Image analysis techniques on evaluation of particle size distribution of gravel. Int J GEOMATE 2012;3:290–7. https://doi.org/10.21660/2012.5.1261.
[21] Rojas J. Rapport de projet interne - Développement d'une méthode pour déterminer la granulométrie du ballast ferroviaire à partir d'images. Riom, France: 2021.
[22] Rojas Vivanco J, Barbier S, Benz Navarrete MA, Breul P. Statistical analysis of the influence of ballast fouling on penetrometer and geoendoscope data. Adv Transp Geotech IV 2021;165:915–30. https://doi.org/10.1007/978-3-030-77234-5_75.
[23] Selig E, Waters J. Track geotechnology and substructure management. Thomas Telford 1994. https://doi.org/10.1680/tgasm.20139.